

Constraining off-shell production of axion-like particles with $Z\gamma$ and WW differential cross-section measurements

Sonia Carrá,¹ Vincent Goumarre,¹ Ruchi Gupta,¹ Sarah Heim,¹ Beate Heinemann,^{1,2} Jan Kuchler,¹ Federico Meloni,¹ Pablo Quilez,¹ and Yee-Chinn Yap¹

¹*Deutsches Elektronen-Synchrotron DESY, 22607 Hamburg, Germany*

²*Physikalisches Institut, Albert-Ludwigs-Universität Freiburg, 79104 Freiburg, Germany*

(Dated: November 29, 2021)

This article describes a search for low-mass axion-like particles (ALPs) at the Large Hadron Collider (LHC). If ALPs were produced at the LHC via gluon-gluon fusion and decayed to bosons, the energy dependence of the measured diboson cross-sections would differ from the Standard Model expectation. Measurements of WW and $Z\gamma$ differential cross-sections by the ATLAS collaboration are interpreted to constrain ALP couplings to W -, Z -bosons and photons assuming gluon-gluon fusion production.

Axions and more generally axion-like particles (ALPs) [1, 2] appear in many extensions of the Standard Model (SM). Often introduced to solve specific questions like the strong CP problem [3–6], they can also be promising dark matter candidates [7–9]. The canonical QCD axion is expected to be extremely light, $m_a \lesssim 10^{-2}$ eV, and feebly interacting, with axion scales out of direct experimental reach, $f_a \gtrsim 10^8$ GeV. However, recently proposed “heavy QCD axions” motivated by the Peccei-Quinn (PQ) quality problem [10–18] may involve scales as low as $f_a \sim \text{TeV}$ [19–36], renewing the interest of collider searches for the axion [37–51].

Searches for ALPs have been performed at many different experiments and cover a large range of masses (m_a) and coupling strengths to SM particles; see Ref. [52] for a recent compilation of results. Following the suggestion of Ref. [47], in this article we explore instead the high-energy tails of differential diboson cross-sections in the search for off-shell production of low-mass ALPs. If $\sqrt{\hat{s}}$ is the energy of the hard-scatter interaction, the cross-section for s -channel production of boson pairs via ALP exchange is expected to increase with \hat{s} , while the SM cross-sections fall with $1/\hat{s}$.

The theoretical framework used throughout this article is a linear effective field theory (EFT), in which electroweak physics beyond the SM (BSM) is described by a linear EFT expansion [53, 54] in terms of towers of gauge invariant operators ordered by their mass dimension. The chosen EFT includes the SM plus an ALP [1, 2, 41], and the scale of the new physics is the ALP decay constant f_a . The EFT approach is only valid if the probed energy is much lower than this scale, i.e. $\sqrt{\hat{s}} \ll f_a$. However, in the applied model the value of f_a only affects the overall cross-section and not the differential distribution, so that the results can easily be scaled to any value of f_a .

The most general CP-conserving effective Lagrangian

describing bosonic ALP couplings reads

$$\mathcal{L} = \frac{1}{2} \partial_\mu a \partial^\mu a + \frac{1}{2} m_a^2 a^2 + \frac{1}{4} g_{agg} a G \tilde{G} + \frac{1}{4} g_{aWW} a W \tilde{W} + \frac{1}{4} g_{aZZ} a Z \tilde{Z} + \frac{1}{4} g_{a\gamma\gamma} a F \tilde{F} + \frac{1}{4} g_{a\gamma Z} a F \tilde{Z}. \quad (1)$$

These bosonic interactions depend solely on three coefficients $c_{\tilde{W}}$, $c_{\tilde{B}}$ and $c_{\tilde{G}}$, which can be directly related to physical interactions and to the coupling parameters [47]:

$$g_{agg} = \frac{4c_{\tilde{G}}}{f_a}, \quad g_{aWW} = \frac{4c_{\tilde{W}}}{f_a} \quad (2)$$

$$g_{a\gamma\gamma} = \frac{4}{f_a} (\sin^2 \theta_W c_{\tilde{W}} + \cos^2 \theta_W c_{\tilde{B}}) \quad (3)$$

$$g_{aZZ} = \frac{4}{f_a} (\sin^2 \theta_W c_{\tilde{B}} + \cos^2 \theta_W c_{\tilde{W}}) \quad (4)$$

$$g_{aZ\gamma} = \frac{8}{f_a} \sin \theta_W \cos \theta_W (c_{\tilde{W}} - c_{\tilde{B}}), \quad (5)$$

where g_{agg} is the coupling strength of the ALP to gluons, $g_{a\gamma\gamma}$ to photons, g_{aWW}/g_{aZZ} to W/Z bosons and $g_{aZ\gamma}$ to a Z boson and a photon. An additional term that couples the ALP to the Higgs field can be introduced in the bosonic Lagrangian inducing a mixing of the ALP with the longitudinal component of the Z boson, and affecting the fermion couplings. For this article the coefficient of this term, $c_{a\phi}$ in Refs. [47, 55], is set to zero [56].

In Ref. [47], diphoton, dijet and ZZ data were used to constrain the parameters g_{agg} , $g_{a\gamma\gamma}$ and g_{aZZ} . In this article, the differential cross-sections for WW and $Z\gamma$ production measured with the ATLAS detector [57–59] are analyzed to constrain g_{aWW} and $g_{aZ\gamma}$. The ALPs are assumed to be produced via the gluon-gluon fusion (ggF) process. In principle other production modes, such as vector-boson fusion, are also possible but are not considered in this article.

In the regime $\hat{s} \gg m_a^2$ and $\hat{s} \gg m_V^2$, the ggF cross-section for non-resonant production of two bosons, V_1 and V_2 , mediated by an ALP, is given by

$$\sigma(V_1 V_2) \propto g_{agg}^2 g_{aV_1 V_2}^2 \hat{s} \quad (6)$$

where g_{agg} is the coupling of the ALP to gluons and $g_{aV_1V_2}$ is the coupling to the two vector bosons of the ALP decay.

Three measurements are interpreted in this article: a WW cross-section measurement with a jet veto ($WW0j$) [57], a WW cross-section measurement with a requirement of at least one jet ($WW1j$) [58] and a $Z\gamma$ cross-section measurement [59]. Only events in which one W boson decays to an electron and an electron neutrino ($e\nu_e$) and the other to a muon and a muon neutrino ($\mu\nu_\mu$) are considered in the WW measurements, while the $Z\gamma$ analysis only includes Z boson decays to electron or muon pairs. Corrections are applied for any experimental effects and the results are presented in fiducial regions defined by the selection criteria in Table I.

The $WW0j$ measurement uses data with an integrated luminosity of 36.1 fb^{-1} . Two leptons are selected with transverse momentum $p_T(\ell) > 27 \text{ GeV}$ and a requirement on the pseudorapidity of $|\eta(\ell)| < 2.5$. Requirements on the invariant mass of the two leptons, $M(\ell\ell)$, and the transverse momentum of the dilepton system, $p_T(\ell\ell)$, are applied to reduce background due to Drell-Yan production, as well as the contribution of Higgs boson decays. The magnitude of the missing transverse momentum, \vec{p}_T^{miss} , is denoted as E_T^{miss} . Events with hadronic jets with $p_T > 35 \text{ GeV}$ and $|\eta| < 4.5$ are vetoed to suppress backgrounds from top quark production. The measurement is performed differentially in six observables.

The $WW1j$ measurement is based on 139 fb^{-1} of data. In addition to kinematic requirements on the leptons and the dilepton system, events are required to have at least one jet with $p_T > 30 \text{ GeV}$ and $|\eta| < 4.5$. The measurement is performed differentially in numerous variables.

Table I: Selection criteria defining the fiducial regions of the $WW0j$, $WW1j$ and $Z\gamma$ cross-section measurements [57–59]. In the $Z\gamma$ analysis the photon must be isolated w.r.t. hadrons in the event, see text and Ref. [57]. Only jets with $|\eta(\text{jet})| < 4.5$ are considered for the jet p_T requirements.

Variable	Selection Cut		
	$WW0j$	$WW1j$	$Z\gamma$
$p_T(\ell)$ [GeV]	> 27	> 27	$> 30, 25$
$ \eta(\ell) $	< 2.5	< 2.5	< 2.47
$M(\ell\ell)$ [GeV]	> 55	> 85	> 40
$p_T(\ell\ell)$ [GeV]	> 30	–	–
E_T^{miss} [GeV]	> 20	–	–
$p_T(\text{jet})$ [GeV]	< 35	> 30	–
$p_T(\gamma)$ [GeV]	–	–	> 30
$ \eta(\gamma) $	–	–	< 2.37
$\Delta R(\ell, \gamma)$	–	–	> 0.4
$M(\ell\ell\gamma) + M(\ell\ell)$ [GeV]	–	–	> 182

The $Z\gamma$ cross-section measurement is also based on 139 fb^{-1} of data, and selects events with a Z boson candidate as well as an isolated photon with high transverse

momentum, $p_T(\gamma) > 30 \text{ GeV}$ and a requirement on the photon pseudorapidity of $|\eta(\gamma)| < 2.37$. A requirement on the sum of the invariant masses of the dilepton system and the $\ell\ell\gamma$ system, $M(\ell\ell\gamma)$, is applied to reduce the contribution from events where the photon is radiated off a lepton. The photon is required to be isolated from hadrons and leptons within a cone defined by $\Delta R = \sqrt{\Delta\eta^2 + \Delta\phi^2}$ where $\Delta\eta$ and $\Delta\phi$ are the differences between the photon and the other particle in pseudo-rapidity and azimuthal angle, respectively. The $Z\gamma$ cross-sections are measured differentially in six observables.

Cross-sections for SM $q\bar{q} \rightarrow WW$ production are determined at next-to-next-to-leading order (NNLO) in QCD, using the parton-level generator MATRIX [60–62], including off-shell effects and the non-resonant and resonant gluon-initiated contributions at LO. For improved precision, the NNLO MATRIX prediction is also complemented with NLO corrections to gluon-induced WW production [63] and with NLO electroweak (EW) corrections that also include the photon-induced contribution [64]. For all predictions the NNPDF 3.1 LUXqed parton distribution function (PDF) set is used [62, 65]. The renormalization and factorization scales are set to half the invariant mass of the W bosons, $M(WW)/2$.

The SM cross-sections for the $\ell\ell\gamma$ process are computed with MATRIX [66] at NNLO in QCD, corrected to particle level using the factors provided in Ref. [59]. The gluon-initiated contributions is included at LO but amounts to only 2%. The cross-sections are obtained with the CT14nnlo PDF set [67], and the transverse momentum (q_T) subtraction method [68]. The values of the renormalisation and factorization scales are set to $\sqrt{M(\ell\ell)^2 + p_T(\gamma)^2}$. Smooth-cone photon isolation [69] is imposed as discussed in Ref. [59]. EW radiative corrections to $Z\gamma$ production have been computed at NLO for the $q\bar{q}$, $q\gamma$ and $\gamma\gamma$ initial states in Refs. [70–72].

The absence of a complete combined calculation of NLO EW and NNLO QCD corrections leads to the question whether the NLO EW corrections associated with the $q\bar{q}$ initial state should be applied multiplicatively or additively to the NNLO QCD corrections. We follow the strategy of the respective publications: For $WW0j$ and $Z\gamma$, the average between the two choices is taken as central value and the difference between the average and either of the choices as the uncertainty, as recommended in Ref. [73]. In the $WW1j$ analysis, the NLO EW corrections are applied multiplicatively and no uncertainty is applied as in the probed phase space the electroweak and QCD corrections should factorize.

Uncertainties on the theoretical predictions due to possible higher order QCD contributions are estimated by varying the renormalisation and factorization scales by factors of up to two. Uncertainties arising from the choice of PDF set and the value of α_s are assessed according to the PDF4LHC recommendations [74] using the 68% con-

fidence level (CL) variations of the NNPDF set [75].

ALP signal events are produced with the MADGRAPH5_aMC@NLO [76] Monte Carlo generator interfaced to PYTHIA 8 [77] for parton showering and hadronization. Samples are produced varying either $c_{\tilde{G}}$, $c_{\tilde{B}}$ or $c_{\tilde{W}}$ for a fixed value of f_a using the set of operators described in Ref. [41]. The following parameters are used unless otherwise stated: $f_a = 1$ TeV and $m_a = 1$ keV. For this analysis the value of m_a is irrelevant as long as $m_a \ll \hat{s}$, and it was explicitly tested that the cross-section is independent of m_a for $m_a < 100$ GeV. The coupling of the axion to gluons, g_{agg} , is in principle an independent free parameter. In the simulation it was set to $g_{agg} = 1$ TeV $^{-1}$ in line with Ref. [47], and some of the results below are presented for this assumption. However, in order to compare the sensitivity of this analysis with constraints from previous experiments, it is assumed that the ratio of the EW axion couplings over the gluonic coupling is controlled by the strength of the corresponding gauge coupling constants, $g_{aV_1V_2}/g_{agg} = \alpha_{V_1V_2}/\alpha_s$ [78]. This assumption is well motivated by pseudo Nambu-Goldstone bosons with anomalous couplings generated by the triangle diagram with $\mathcal{O}(1)$ group theory factors, see e.g. Ref. [46].

In the $\ell\ell\gamma$ final state, only $a \rightarrow Z\gamma$ is considered. In principle there is also a contribution from $\gamma^*\gamma$ but based on the constraints already set in Ref. [41] it is negligible. The A14 tune is used for the modeling of parton showering, the hadronization and the underlying event. Parton luminosities are provided by the NNPDF2.3LO PDF set. The LO cross-section from the generator prediction is used. It is worth noting that it is likely that there are large NLO corrections, similar to the factor of ~ 2 found for ggF production of the Higgs boson, and accounting for these would result in more stringent constraints than those presented here. For the ALP predictions no theoretical uncertainties are considered.

The fiducial selections of the WW and $Z\gamma$ cross-section measurements shown in Table I are applied to the generated ALP events using RIVET analysis routines [79]. Interference between the SM and the ALP process is neglected. For the $WW0j$ channel, 17% of all $a \rightarrow WW \rightarrow e\nu\mu\nu$ events pass the fiducial selection. Most of the inefficiency arises from the jet veto which rejects nearly 75% of the ALP events. For the $WW1j$ channel, the fraction of $a \rightarrow WW \rightarrow e\nu\mu\nu$ events passing the fiducial selection is 45%. In the $Z\gamma$ channel, 55% of all $a \rightarrow Z\gamma \rightarrow \ell^+\ell^-\gamma$ ($\ell = e$ and μ) events are selected.

The measured cross-section in each bin is compared to the sum of the SM and varying ALP contributions. The predictions and the measured cross-sections are used to construct a binned likelihood function \mathcal{L} based on a product of Poisson probability terms over all bins of the differential cross-section distribution. This function depends on the product of coupling parameters, $g_{aV_1V_2} \times g_{agg}$, and a set of nuisance parameters θ that encode the ef-

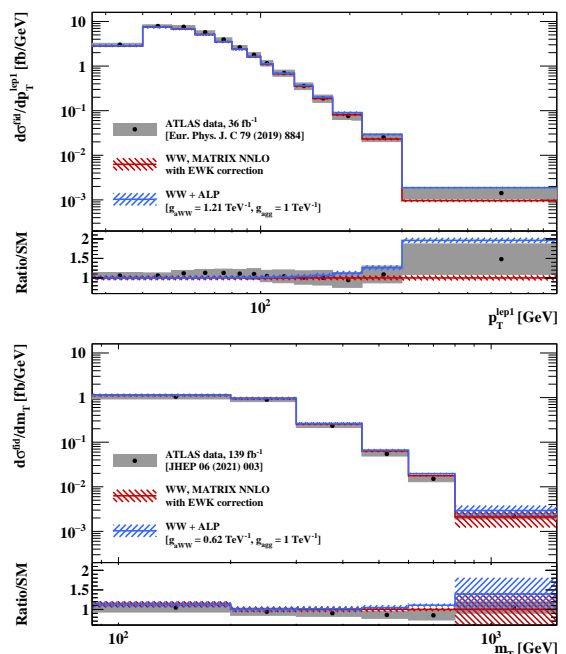


Figure 1: Differential cross-sections as a function of (top) the leading lepton p_T measured in $WW0j$ events, (bottom) the transverse mass m_T measured in $WW1j$ events. The data is compared to the SM prediction and a hypothetical ALP signal with $m_a = 1$ keV, $f_a = 1$ TeV, $g_{agg} = 1$ TeV $^{-1}$, and g_{aWW} as shown in the legend corresponding to the derived 95% CL upper limit in each analysis. The lower panels show the ratios of the data and of the sum of SM and ALP contribution to the SM prediction.

fect of systematic uncertainties in the signal and background expectations. All experimental uncertainties on the measurements as documented in Ref. [57–59] and the uncertainties on the SM predictions related to PDFs and higher order QCD/EW corrections as discussed above, are incorporated as nuisance parameters with Gaussian constraints.

The sensitivity to $g_{aV_1V_2} \times g_{agg}$ is studied for each of the measured observables using pseudo-experiments. It is evaluated by determining the expected upper limits on the relevant ALP coupling parameters.

For $WW0j$ production, the p_T of the leading lepton provides the best sensitivity, while for $WW1j$ production the transverse mass of the dilepton system and E_T^{miss} , $m_T = \sqrt{(p_T(\ell\ell) + E_T^{\text{miss}})^2 - (\vec{p}_T(\ell\ell) + \vec{p}_T^{\text{miss}})^2}$ is the most sensitive observable. For $Z\gamma$, the photon p_T is the strongest discriminator. The distributions are shown in Fig. 1 and Fig. 2, compared to the SM prediction and to the sum of the prediction for the SM and a hypothetical ALP signal, for the WW and $Z\gamma$ analyses, respectively.

The likelihood fits to the data show no significant de-

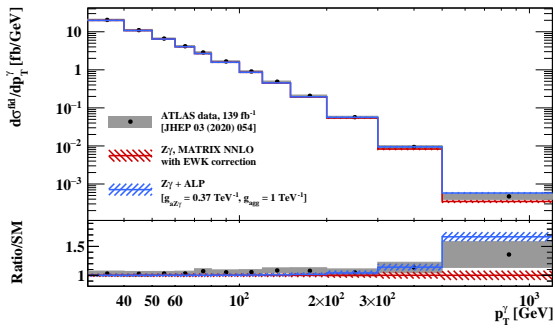


Figure 2: Differential cross-sections as a function of the photon p_T measured in $Z\gamma$ events. The data is compared to the SM prediction and a hypothetical ALP signal with $m_a = 1$ keV, $f_a = 1$ TeV, $g_{agg} = 1$ TeV $^{-1}$, and g_{aWW} and $g_{aZ\gamma}$ as shown in the legend corresponding to the derived 95% CL upper limit of the analysis. The lower panels show the ratios of the data and of the sum of SM and ALP contribution to the SM prediction.

viation from the SM predictions: The central values for both the WW and the $Z\gamma$ coupling of the ALP are consistent with 0 within $< 1.5\sigma$. The observed and expected limits on the coupling parameters at the 95% CL are given in Table II. The expected upper limit of the $WW1j$ analysis is about a factor two better than that of the $WW0j$ analysis.

While the data constrain the product, $g_{agg}g_{aVV}$, in Table II constraints on g_{aVV} are presented for a fixed value of $g_{agg} = 1$ TeV $^{-1}$. They can trivially be converted into limits on the product of the couplings $g_{agg}g_{aWW}$ and $g_{agg}g_{aZ\gamma}$: the observed upper limits are $g_{aWW} < 0.62$ TeV $^{-2}$ and $g_{aZ\gamma} < 0.37$ TeV $^{-2}$ at 95% CL, respectively.

Table II: Observed (obs.) and expected (exp.) 95% CL upper limits on the coupling parameters g_{aWW} and $g_{aZ\gamma}$ based on the fit to the $WW0j$, $WW1j$ and $Z\gamma$ data assuming $g_{agg} = 1$ TeV $^{-1}$, respectively. Also given are the corresponding constraints on $c_{\tilde{W}}$ and $c_{\tilde{W}} - c_{\tilde{B}}$ for $f_a = 1$ TeV.

Parameter	Analysis	$\int \mathcal{L} dt$ [fb $^{-1}$]	95% CL upper limit	
			obs.	exp.
g_{aWW} [TeV $^{-1}$]	$WW0j$, $p_T^{\ell 1}$	36	1.21	1.00
g_{aWW} [TeV $^{-1}$]	$WW1j$, m_T	139	0.62	0.49
$g_{aZ\gamma}$ [TeV $^{-1}$]	$Z\gamma$, $p_T^{\ell 1}$	139	0.37	0.29
$ c_{\tilde{W}} $	$WW0j$, $p_T^{\ell 1}$	36	0.30	0.25
$ c_{\tilde{W}} $	$WW1j$, m_T	139	0.15	0.12
$ c_{\tilde{W}} - c_{\tilde{B}} $	$Z\gamma$, $p_T^{\ell 1}$	139	0.11	0.09

Based on Eq. 2, and assuming a value for f_a , the limits on the coupling parameters can be translated to constraints on the coefficients $c_{\tilde{W}}$ and $c_{\tilde{B}}$, as shown in Table II. The value of $f_a = 1$ TeV is chosen so that

the results can be compared directly to those derived in Ref. [47] from ZZ and $\gamma\gamma$ measurements. It is worth noting that the choice of $f_a = 1$ TeV is rather controversial as f_a is the scale of new physics and the data used here actually probe that regime directly, making the usage of the EFT questionable. Since the choice of f_a only affects the coupling strength and does not affect the kinematic distributions, the $c_{\tilde{W}}$ and $c_{\tilde{B}}$ values can easily be rescaled to any f_a value. For instance, for $f_a = 5$ TeV the values of the upper limits on the coefficients are five times higher.

It was also tested how the expected upper limits of the $WW0j$ and $WW1j$ compare when using the same method and the same luminosity. Using the $p_T^{\ell 1}$ distribution and an integrated luminosity of 139 fb $^{-1}$ for both gives an expected limit of $|c_{\tilde{W}}| < 0.20$ for the $WW0j$ and $|c_{\tilde{W}}| < 0.16$ for the $WW1j$ analysis. While the $WW1j$ provides a slightly stronger constraint, a statistical combination of the two results would likely yield improved results and could be considered in the future. The expected limit for the $WW1j$ analysis of $|c_{\tilde{W}}| < 0.16$ based on $p_T^{\ell 1}$ is a factor 1.25 larger than that obtained based on m_T , shown in Table II. Thus m_T was used for the data interpretation.

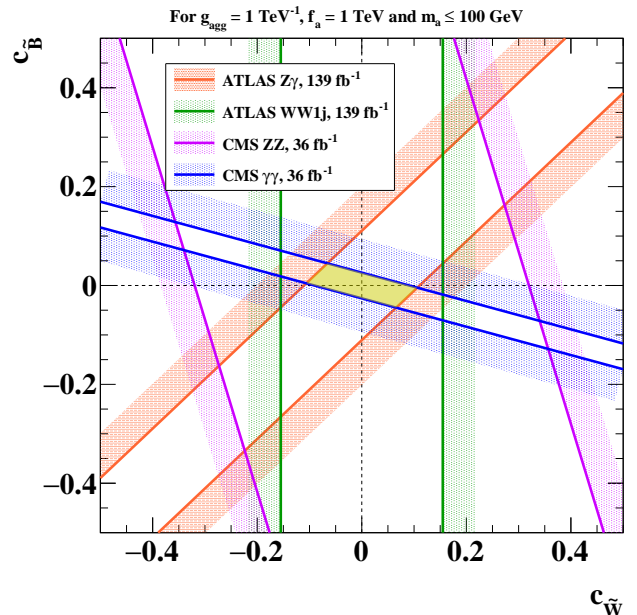


Figure 3: 95% CL constraints on $c_{\tilde{W}}$ and $c_{\tilde{B}}$ from this work ($Z\gamma$ and WW) and from Ref. [47] (ZZ and $\gamma\gamma$). Values of $g_{agg} = 1$ TeV $^{-1}$, $f_a = 1$ TeV and $m_a = 1$ keV are assumed. The yellow area is still allowed by all analyses.

The observed upper limits on the coefficients $c_{\tilde{B}}$ and $c_{\tilde{W}}$ for $f_a = 1$ TeV are displayed in Fig. 3 for four analyses: $\gamma\gamma$ and ZZ from Ref. [47], and $WW1j$ and $Z\gamma$ from the present analysis. The WW process is independent of

$c_{\tilde{B}}$ while the other three processes depend on both $c_{\tilde{W}}$ and $c_{\tilde{B}}$ with different dependencies. When considering all four constraints only the small area near zero is allowed with $|c_{\tilde{W}}| < 0.11$ and $|c_{\tilde{B}}| < 0.045$. This area is constrained just by the $\gamma\gamma$ and $Z\gamma$ processes, and the WW and ZZ processes add no further information in this model.

In Fig. 4 the constraints derived in this analysis on g_{aWW} and $g_{aZ\gamma}$ are compared to those from other experiments, see Ref. [46] and references therein. For this purpose, the assumption is made that g_{agg} is related to the coupling to EW vector-bosons via the gauge coupling strengths, $g_{aV_1V_2}/g_{agg} = \alpha_{V_1V_2}/\alpha_s$ as discussed above. The constraints labelled ‘‘Photons’’ are based on beam dump experiments, supernova SN1987a observations, as well as LHC results. Due to radiative corrections of the axion-boson couplings to the axion-photon couplings, these results can be converted to constraints on g_{aWW} and $g_{aZ\gamma}$, assuming only a very mild dependence on f_a [46]. For the constraints labelled ‘‘LHC’’, it is assumed that g_{agg} is much larger than g_{aWW} or $g_{aZ\gamma}$, eliminating much of the dependence on the gluon coupling [46]. The LHC bound on $g_{aZ\gamma}$ for low masses has been updated with respect to Ref. [46] with the recent results on $Z \rightarrow \gamma + \text{inv}$ by ATLAS [80]. For reference purposes, the QCD axion line is shown in black assuming $\mathcal{O}(1)$ anomaly factors [81]

For the g_{aWW} coupling, the present analysis closes a gap in the coverage in the mass range between 0.4 GeV and 100 GeV which was a challenging region of masses since previous analyses studying solely EW axion couplings are no longer applicable in the presence of a gluonic coupling for masses above $m_a > 3m_\pi$ due to the opening of the hadronic decay channel. For the $g_{aZ\gamma}$, a lot of the mass range covered by this analysis was already excluded by LEP analyses but this analysis extends to lower couplings by up to an order of magnitude.

We have evaluated recent ATLAS cross-section measurements of WW and $Z\gamma$ in the search for off-shell production of low-mass axion-like particles. Such particles would alter the spectrum at high energies. In the absence of any significant excesses the measurements allow to constrain interactions of axion-like particles with EW and strong gauge bosons. Together with the previous constraints based on the analysis of $\gamma\gamma$ data from Ref. [47], the presented analysis provides strong constraints on the coupling parameters of the linear bosonic ALP EFT. The constraints presented here are the strongest to date in the mass range $m_a \sim (0.4 - 100)$ GeV for both the aWW and the $aZ\gamma$ coupling for the parameter ranges considered.

ACKNOWLEDGEMENTS

We thank B. Gavela and V. Sanz for the inspiration for this analysis, the useful discussions and for making the

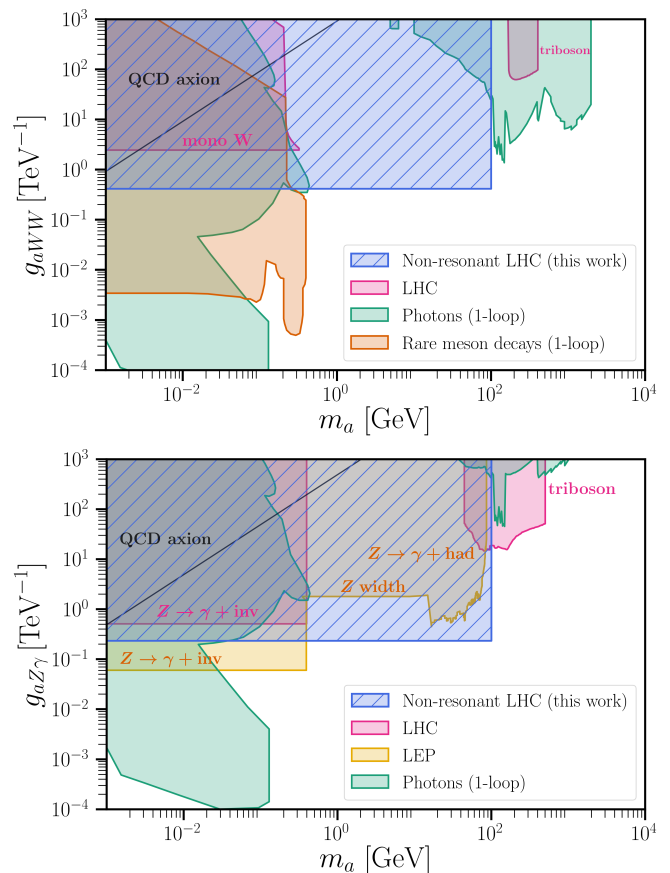


Figure 4: 95% CL constraints on g_{aWW} (top) and $g_{aZ\gamma}$ (bottom). The constraints derived in this work are shown as the hatched area. Also shown are constraints from other experiments, see text.

ALPs EFT UFO models available for use. We also thank Gonzalo Alonso-Álvarez for providing us the data of the combined previous bounds. The work by V. Goumarre, B. Heinemann, S. Heim and P. Quílez was in part funded by the Deutsche Forschungsgemeinschaft under Germany’s Excellence Strategy - EXC 2121 ‘‘Quantum Universe’’ - 390833306. S. Heim thanks the Helmholtz Association for the support through the ‘‘Young Investigator Group’’ initiative. This work has benefited from computing services provided by the German National Analysis Facility (NAF).

- [1] H. Georgi, D. B. Kaplan, and L. Randall, ‘‘Manifesting the Invisible Axion at Low-energies,’’ *Phys. Lett. B*, vol. 169, pp. 73–78, 1986.
- [2] K. Choi, K. Kang, and J. E. Kim, ‘‘Effects of η' in Low-energy Axion Physics,’’ *Phys. Lett. B*, vol. 181, pp. 145–149, 1986.
- [3] R. D. Peccei and H. R. Quinn, ‘‘CP Conservation in the Presence of Instantons,’’ *Phys. Rev. Lett.*, vol. 38,

- pp. 1440–1443, 1977.
- [4] R. D. Peccei and H. R. Quinn, “Constraints Imposed by CP Conservation in the Presence of Instantons,” *Phys. Rev. D*, vol. 16, pp. 1791–1797, 1977.
- [5] S. Weinberg, “A New Light Boson?,” *Phys. Rev. Lett.*, vol. 40, pp. 223–226, 1978.
- [6] F. Wilczek, “Problem of Strong P and T Invariance in the Presence of Instantons,” *Phys. Rev. Lett.*, vol. 40, pp. 279–282, 1978.
- [7] J. Preskill, M. B. Wise, and F. Wilczek, “Cosmology of the Invisible Axion,” *Phys. Lett. B*, vol. 120, pp. 127–132, 1983.
- [8] L. F. Abbott and P. Sikivie, “A Cosmological Bound on the Invisible Axion,” *Phys. Lett. B*, vol. 120, pp. 133–136, 1983.
- [9] M. Dine and W. Fischler, “The Not So Harmless Axion,” *Phys. Lett. B*, vol. 120, pp. 137–141, 1983.
- [10] R. Holman, S. D. H. Hsu, T. W. Kephart, E. W. Kolb, R. Watkins, and L. M. Widrow, “Solutions to the strong CP problem in a world with gravity,” *Phys. Lett. B*, vol. 282, pp. 132–136, 1992.
- [11] M. Kamionkowski and J. March-Russell, “Planck scale physics and the Peccei-Quinn mechanism,” *Phys. Lett. B*, vol. 282, pp. 137–141, 1992.
- [12] S. M. Barr and D. Seckel, “Planck scale corrections to axion models,” *Phys. Rev. D*, vol. 46, pp. 539–549, 1992.
- [13] S. Ghigna, M. Lusignoli, and M. Roncadelli, “Instability of the invisible axion,” *Phys. Lett. B*, vol. 283, pp. 278–281, 1992.
- [14] H. M. Georgi, L. J. Hall, and M. B. Wise, “Grand Unified Models With an Automatic Peccei-Quinn Symmetry,” *Nucl. Phys. B*, vol. 192, pp. 409–416, 1981.
- [15] S. B. Giddings and A. Strominger, “Loss of Incoherence and Determination of Coupling Constants in Quantum Gravity,” *Nucl. Phys. B*, vol. 307, pp. 854–866, 1988.
- [16] S. R. Coleman, “Why There Is Nothing Rather Than Something: A Theory of the Cosmological Constant,” *Nucl. Phys. B*, vol. 310, pp. 643–668, 1988.
- [17] G. Gilbert, “WORMHOLE INDUCED PROTON DECAY,” *Nucl. Phys. B*, vol. 328, pp. 159–170, 1989.
- [18] S.-J. Rey, “The Axion Dynamics in Wormhole Background,” *Phys. Rev. D*, vol. 39, p. 3185, 1989.
- [19] V. A. Rubakov, “Grand unification and heavy axion,” *JETP Lett.*, vol. 65, pp. 621–624, 1997.
- [20] Z. Berezhiani, L. Gianfagna, and M. Giannotti, “Strong CP problem and mirror world: The Weinberg-Wilczek axion revisited,” *Phys. Lett. B*, vol. 500, pp. 286–296, 2001.
- [21] L. Gianfagna, M. Giannotti, and F. Nesti, “Mirror world, supersymmetric axion and gamma ray bursts,” *JHEP*, vol. 10, p. 044, 2004.
- [22] S. D. H. Hsu and F. Sannino, “New solutions to the strong CP problem,” *Phys. Lett. B*, vol. 605, pp. 369–375, 2005.
- [23] A. Hook, “Anomalous solutions to the strong CP problem,” *Phys. Rev. Lett.*, vol. 114, no. 14, p. 141801, 2015.
- [24] H. Fukuda, K. Harigaya, M. Ibe, and T. T. Yanagida, “Model of visible QCD axion,” *Phys. Rev. D*, vol. 92, no. 1, p. 015021, 2015.
- [25] C.-W. Chiang, H. Fukuda, M. Ibe, and T. T. Yanagida, “750 GeV diphoton resonance in a visible heavy QCD axion model,” *Phys. Rev. D*, vol. 93, no. 9, p. 095016, 2016.
- [26] S. Dimopoulos, A. Hook, J. Huang, and G. Marques-Tavares, “A collider observable QCD axion,” *JHEP*, vol. 11, p. 052, 2016.
- [27] T. Gherghetta, N. Nagata, and M. Shifman, “A Visible QCD Axion from an Enlarged Color Group,” *Phys. Rev. D*, vol. 93, no. 11, p. 115010, 2016.
- [28] A. Kobakhidze, “Heavy axion in asymptotically safe QCD,” 7 2016.
- [29] P. Agrawal and K. Howe, “Factoring the Strong CP Problem,” *JHEP*, vol. 12, p. 029, 2018.
- [30] P. Agrawal and K. Howe, “A Flavorful Factoring of the Strong CP Problem,” *JHEP*, vol. 12, p. 035, 2018.
- [31] M. K. Gaillard, M. B. Gavela, R. Houtz, P. Quilez, and R. Del Rey, “Color unified dynamical axion,” *Eur. Phys. J. C*, vol. 78, no. 11, p. 972, 2018.
- [32] M. A. Buen-Abad and J. Fan, “Dynamical axion misalignment with small instantons,” *JHEP*, vol. 12, p. 161, 2019.
- [33] C. Csáki, M. Ruhdorfer, and Y. Shirman, “UV Sensitivity of the Axion Mass from Instantons in Partially Broken Gauge Groups,” *JHEP*, vol. 04, p. 031, 2020.
- [34] R. S. Gupta, V. V. Khoze, and M. Spannowsky, “Small instantons and the strong CP problem in composite Higgs models,” 11 2020.
- [35] T. Gherghetta and M. D. Nguyen, “A Composite Higgs with a Heavy Composite Axion,” *JHEP*, vol. 12, p. 094, 2020.
- [36] F. Takahashi and W. Yin, “Heavy QCD axion inflation,” 5 2021.
- [37] J. Jaeckel and M. Spannowsky, “Probing MeV to 90 GeV axion-like particles with LEP and LHC,” *Phys. Lett. B*, vol. 753, pp. 482–487, 2016.
- [38] K. Mimasu and V. Sanz, “ALPs at Colliders,” *JHEP*, vol. 06, p. 173, 2015.
- [39] M. Bauer, M. Neubert, and A. Thamm, “Collider Probes of Axion-Like Particles,” *JHEP*, vol. 12, p. 044, 2017.
- [40] M. Bauer, M. Heiles, M. Neubert, and A. Thamm, “Axion-Like Particles at Future Colliders,” *Eur. Phys. J. C*, vol. 79, no. 1, p. 74, 2019.
- [41] I. Brivio, M. B. Gavela, L. Merlo, K. Mimasu, J. M. No, R. del Rey, and V. Sanz, “ALPs Effective Field Theory and Collider Signatures,” *Eur. Phys. J. C*, vol. 77, no. 8, p. 572, 2017.
- [42] N. Craig, A. Hook, and S. Kasko, “The Photophobic ALP,” *JHEP*, vol. 09, p. 028, 2018.
- [43] X. Cid Vidal, A. Mariotti, D. Redigolo, F. Sala, and K. Tobioka, “New Axion Searches at Flavor Factories,” *JHEP*, vol. 01, p. 113, 2019. [Erratum: *JHEP* 06, 141 (2020)].
- [44] E. Izaguirre, T. Lin, and B. Shuve, “Searching for Axion-like Particles in Flavor-Changing Neutral Current Processes,” *Phys. Rev. Lett.*, vol. 118, no. 11, p. 111802, 2017.
- [45] M. Freytsis, Z. Ligeti, and J. Thaler, “Constraining the Axion Portal with $B \rightarrow K l^+ l^-$,” *Phys. Rev. D*, vol. 81, p. 034001, 2010.
- [46] G. Alonso-Álvarez, M. B. Gavela, and P. Quilez, “Axion couplings to electroweak gauge bosons,” *Eur. Phys. J. C*, vol. 79, no. 3, p. 223, 2019.
- [47] M. B. Gavela, J. M. No, V. Sanz, and J. F. de Trocóniz, “Nonresonant Searches for Axionlike Particles at the LHC,” *Phys. Rev. Lett.*, vol. 124, no. 5, p. 051802, 2020.
- [48] A. Hook, S. Kumar, Z. Liu, and R. Sundrum, “High Quality QCD Axion and the LHC,” *Phys. Rev. Lett.*, vol. 124, no. 22, p. 221801, 2020.

- [49] G. Haghhighat, D. Haji Raissi, and M. Mohammadi Najafabadi, “New collider searches for axionlike particles coupling to gluons,” *Phys. Rev. D*, vol. 102, no. 11, p. 115010, 2020.
- [50] G. Alonso-Álvarez, F. Ertas, J. Jaeckel, F. Kahlhoefer, and L. J. Thormaehlen, “Leading logs in QCD axion effective field theory,” *JHEP*, vol. 07, p. 059, 2021.
- [51] S. Chakraborty, M. Kraus, V. Loladze, T. Okui, and K. Tobioka, “Heavy QCD axion in $b \rightarrow s$ transition: Enhanced limits and projections,” *Phys. Rev. D*, vol. 104, no. 5, p. 055036, 2021.
- [52] R. K. Ellis et al., “Physics Briefing Book: Input for the European Strategy for Particle Physics Update 2020.” arXiv:1910.11775.
- [53] W. Buchmuller and D. Wyler, “Effective Lagrangian Analysis of New Interactions and Flavor Conservation,” *Nucl. Phys. B*, vol. 268, pp. 621–653, 1986.
- [54] B. Grzadkowski, M. Iskrzynski, M. Misiak, and J. Rosiek, “Dimension-Six Terms in the Standard Model Lagrangian,” *JHEP*, vol. 10, p. 085, 2010.
- [55] M. B. Gavela, R. Houtz, P. Quilez, R. Del Rey, and O. Sumensari, “Flavor constraints on electroweak ALP couplings,” *Eur. Phys. J. C*, vol. 79, no. 5, p. 369, 2019.
- [56] It was also tested that for $c_{a\phi} = 1$ the same results are obtained.
- [57] ATLAS Collaboration, “Measurement of fiducial and differential W^+W^- production cross-sections at $\sqrt{s} = 13$ TeV with the ATLAS detector,” *Eur. Phys. J. C*, vol. 79, no. 10, p. 884, 2019.
- [58] ATLAS Collaboration, “Measurements of $W^+W^- + \geq 1$ jet production cross-sections in pp collisions at $\sqrt{s} = 13$ TeV with the ATLAS detector,” *JHEP*, vol. 06, p. 003, 2021.
- [59] ATLAS Collaboration, “Measurement of the $Z(\rightarrow \ell^+\ell^-)\gamma$ production cross-section in pp collisions at $\sqrt{s} = 13$ TeV with the ATLAS detector,” *JHEP*, vol. 03, p. 054, 2020.
- [60] T. Gehrmann, A. von Manteuffel, and L. Tancredi, “The two-loop helicity amplitudes for $q\bar{q}' \rightarrow V_1V_2 \rightarrow 4$ leptons,” *JHEP*, vol. 09, p. 128, 2015.
- [61] F. Cascioli, P. Maierhofer, and S. Pozzorini, “Scattering Amplitudes with Open Loops,” *Phys. Rev. Lett.*, vol. 108, p. 111601, 2012.
- [62] R. D. Ball et al., “Parton distributions from high-precision collider data,” *Eur. Phys. J. C*, vol. 77, no. 10, p. 663, 2017.
- [63] F. Caola, M. Dowling, K. Melnikov, R. Röntsch, and L. Tancredi, “QCD corrections to vector boson pair production in gluon fusion including interference effects with off-shell Higgs at the LHC,” *JHEP*, vol. 07, p. 087, 2016.
- [64] B. Biedermann, M. Billoni, A. Denner, S. Dittmaier, L. Hofer, B. Jäger, and L. Salfelder, “Next-to-leading-order electroweak corrections to $pp \rightarrow W^+W^- \rightarrow 4$ leptons at the LHC,” *JHEP*, vol. 06, p. 065, 2016.
- [65] V. Bertone, S. Carrazza, N. P. Hartland, and J. Rojo, “Illuminating the photon content of the proton within a global PDF analysis,” *SciPost Phys.*, vol. 5, no. 1, p. 008, 2018.
- [66] M. Grazzini, S. Kallweit, and M. Wiesemann, “Fully differential NNLO computations with MATRIX,” *Eur. Phys. J. C*, vol. 78, no. 7, p. 537, 2018.
- [67] S. Dulat, T.-J. Hou, J. Gao, M. Guzzi, J. Huston, P. Nadolsky, J. Pumplin, C. Schmidt, D. Stump, and C. P. Yuan, “New parton distribution functions from a global analysis of quantum chromodynamics,” *Phys. Rev. D*, vol. 93, no. 3, p. 033006, 2016.
- [68] S. Catani and M. Grazzini, “Next-to-next-to-leading-order subtraction formalism in hadron collisions and its application to higgs-boson production at the large hadron collider,” *Phys. Rev. Lett.*, vol. 98, p. 222002, May 2007.
- [69] S. Frixione, “Isolated photons in perturbative QCD,” *Phys. Lett. B*, vol. 429, pp. 369–374, 1998.
- [70] A. Denner, S. Dittmaier, M. Hecht, and C. Pasold, “NLO QCD and electroweak corrections to $Z + \gamma$ production with leptonic Z-boson decays,” *JHEP*, vol. 02, p. 057, 2016.
- [71] W. Hollik and C. Meier, “Electroweak corrections to gamma Z production at hadron colliders,” *Phys. Lett. B*, vol. 590, pp. 69–75, 2004.
- [72] E. Accomando, A. Denner, and C. Meier, “Electroweak corrections to $W\gamma$ and $Z\gamma$ production at the LHC,” *Eur. Phys. J. C*, vol. 47, pp. 125–146, 2006.
- [73] M. Grazzini, S. Kallweit, J. M. Lindert, S. Pozzorini, and M. Wiesemann, “NNLO QCD + NLO EW with Matrix+OpenLoops: precise predictions for vector-boson pair production,” *JHEP*, vol. 02, p. 087, 2020.
- [74] J. Butterworth et al., “PDF4LHC recommendations for LHC Run II,” *J. Phys. G*, vol. 43, p. 023001, 2016.
- [75] R. D. Ball et al., “Parton distributions for the LHC Run II,” *JHEP*, vol. 04, p. 040, 2015.
- [76] J. Alwall, R. Frederix, S. Frixione, V. Hirschi, F. Maltoni, O. Mattelaer, H. S. Shao, T. Stelzer, P. Torrielli, and M. Zaro, “The automated computation of tree-level and next-to-leading order differential cross sections, and their matching to parton shower simulations,” *JHEP*, vol. 07, p. 079, 2014.
- [77] T. Sjöstrand, S. Ask, J. R. Christiansen, R. Corke, N. Desai, P. Ilten, S. Mrenna, S. Prestel, C. O. Rasmussen, and P. Z. Skands, “An introduction to PYTHIA 8.2,” *Comput. Phys. Commun.*, vol. 191, p. 159, 2015.
- [78] $\alpha_{V_1V_2}$ is defined as $\alpha_{em} = \alpha_{WW} s_w^2 = \alpha_{Z\gamma} s_w c_w$, where s_w and c_w denote the sine and cosine of the weak mixing angle.
- [79] C. Bierlich et al., “Robust Independent Validation of Experiment and Theory: Rivet version 3,” *SciPost Phys.*, vol. 8, p. 026, 2020.
- [80] G. Aad et al., “Search for dark matter in association with an energetic photon in pp collisions at $\sqrt{s} = 13$ TeV with the ATLAS detector,” *JHEP*, vol. 02, p. 226, 2021.
- [81] i.e. $g_{aWW} = (\alpha_{em}/s_w^2)/(2\pi f_a)$ and $g_{aZ\gamma} = (\alpha_{em}/s_w c_w)/(2\pi f_a)$.